**Project Report**
**NASA/A-6**

# An Exploratory Study of Modeling Enroute Pilot Convective Storm Flight Deviation Behavior


**R. DeLaura**
**J. Evans**


**May 11, 2006**


**Lincoln Laboratory**

**MASSACHUSETTS INSTITUTE OF TECHNOLOGY**

***Lexington, Massachusetts***



**Prepared for the National Aeronautics and Space Administration**
**Langley Research Center**
**Hampton, VA 23681**

# ABSTRACT

This report presents the results of the Convective Storm Flight Deviation study, funded by the National Aeronautics and Space Administration (NASA) Strategic Airspace Usage (SAU) project under Air Force Contract No. FA8721-05-C-0002. A quantitative model to predict pilot deviations around convective weather in enroute airspace was developed. The model is based on the analysis of planned and actual flight trajectories and the weather encountered along them in two different Air Traffic Control “super-sectors” (geographical regions that include several adjacent ATC enroute sectors) on five different days in the summer of 2003. One super-sector encompassed southern Indiana, southwestern Ohio and northern Kentucky (ZID); the other was located in northern Ohio, along the southern shore of Lake Erie (ZOB).

A deviation distance threshold for each super-sector was determined by analyzing the differences between planned and actual trajectories during a 24-hour period in which no significant weather was present in either super-sector. A method was developed to detect automatically planned and actual flight trajectories that encountered significant weather and to determine which of these encounters were weather-related flight path deviations. The results of the automatic detection algorithm were verified by an analyst, and the verified detection results (weather-related deviations and penetrations) and associated weather statistics provided input to statistical classification algorithms that were used to generate the deviation model.

More than 800 flights whose planned trajectories encountered significant weather were analyzed in the study. The weather was characterized by the Corridor Integrated Weather System (CIWS) high-resolution precipitation (VIL) and radar echo tops products, which are more accurate than weather products used in earlier storm flight deviation studies. ‘Significant’ weather was defined as *either* precipitation greater than or equal to VIP level 2 *or* echo top height greater than or equal to 25 kft.

The study also presents an analysis of several “avoidance distances” associated with deviations. The avoidance distance is defined as the minimum distance between the deviating flight trajectory and the boundary of a particular weather feature (for example, the 30,000 foot echo top contour). Avoidance distances were calculated for 24 different weather feature boundaries from more than 200 deviations selected by an analyst.

Finally, weather penetration statistics are presented for all five case days studied.

In the ZID super-sector, where convective cells were generally characterized by high VIL, high echo tops and clear boundaries, and clear air routes showed little variation, deviation detection and prediction results were as follows:

1. The automated deviation detection algorithm achieved approximately 90% probability of detection and 10% false alarm rate for both deviations and non-deviations when planned trajectories encountered significant weather.

2. The best predictor of weather-related deviation is *deltaZ* (the difference between flight altitude and radar echo top) along the planned flight trajectory. Deviation prediction models based on deltaZ and VIL or deltaZ and lightning counts encountered along the planned trajectory performed equally well, with prediction error rates of approximately 22%.

3. More than 70% of pilots whose planned flight trajectories encountered convective cells with tops at least 6 kft below flight altitude flew over the top of the cells and did not deviate.

4. Pilots deviating around convective cells flew within 25 km of cell boundaries (VIP level 3 contour around the convective cell) in approximately 75% of deviations analyzed.

In the ZOB super-sector, where the weather was generally characterized by low-topped, weak convection and clear air routes showed greater variation, neither the automated deviation detection algorithm nor a human analyst could easily identify weather-related deviations. As a result, a deviation prediction model could not be developed for ZOB.

# TABLE OF CONTENTS


| | | Page |
|---|---|---|
| | ABSTRACT | iii |
| | LIST OF ILLUSTRATIONS | vii |
| | LIST OF TABLES | ix |
| 1. | INTRODUCTION | 1 |
| 2. | ANALYSIS METHODS | 3 |
| 3. | RESULTS | 7 |
| | 3.1 Case Analysis | 7 |
| | 3.2 Deviation Prediction Model | 13 |
| | 3.3 Avoidance Distance Analysis | 19 |
| | 3.4 Weather Penetration | 21 |
| 4. | SUMMARY, CONCLUSIONS AND ADDITIONAL WORK | 23 |
| APPENDIX A | WEATHER STATISTICS USED TO CHARACTERIZE CONVECTIVE WEATHER | 27 |
| APPENDIX B | DEVIATION MODELING | 31 |
| APPENDIX C | CONVECTIVE FEATURE BOUNDARIES AND DETERMINATION OF AVOIDANCE DISTANCE | 39 |
| GLOSSARY | | 43 |
| REFERENCES | | 45 |

# LIST OF ILLUSTRATIONS


| Figure No. | | Page |
|---|---|---|
| 1 | Illustration of different neighborhood scales used in the extraction of weather data and calculation of weather statistics for weather encounters along planned and actual flight trajectories. | 4 |
| 2 | Jetways and clear day traffic in super-sectors ZOB and ZID. | 7 |
| 3 | Deviation threshold analysis in ZID and ZOB super-sectors. | 8 |
| 4 | A typical storm cell deviation in the ZID super-sector. | 10 |
| 5 | A typical storm cell deviation in the ZID super-sector. | 10 |
| 6 | A typical weather-related deviation in the ZOB super-sector. | 11 |
| 7 | A typical weather-related deviation in the ZOB super-sector. | 12 |
| 8 | Summary of deviation prediction model errors. | 15 |
| 9 | 2D histograms of deviation counts (a), non-deviation counts (b), observed probability of deviation (percentage of flights in each histogram bin that deviated) (c) and a smoothed probability function derived from the observed probabilities (d). | 16 |
| 10 | Relationship between weather inputs and deviation / non-deviation result. | 17 |
| 11 | Deviation decision plot, as a function of weather input variables. | 18 |
| 12 | Histograms of lightning counts within the 60km encounter neighborhood box in the 6 minutes immediately prior to weather encounters in ZID and ZOB. | 19 |
| 13 | Avoidance distance analysis. | 19 |
| 14 | Illustration of unclear deviation strategy. | 20 |
| 15 | ZID penetrations. | 32 |
| 16 | ZOB penetrations. | 22 |

# LIST OF ILLUSTRATIONS
## (Continued)


| Figure No. | | Page |
|---|---|---|
| B-1 | Illustration of predictor strength. | 32 |
| B-2 | Deviation prediction errors corresponding to Table B1. | 35 |
| B-3 | Deviation prediction errors corresponding to Table B2. | 36 |
| B-4 | Deviation prediction errors corresponding to Table B3. | 38 |
| C-1 | Distribution of weather feature avoidance distances. | 39 |

# LIST OF TABLES


| Table No. | | Page |
|---|---|---|
| 1 | Summary of Weather Encounters for Planned Trajectories | 9 |
| 2 | Summary of Automated Deviation Detection Algortihm Performance | 13 |
| A-1 | VIL to Interest Level Mapping | 27 |
| A-2 | Weather Statistics Used to Characterize Weather Encounters along Planned and Actual Flight Trajectories | 28 |
| B-1 | Summary of deviation prediction model experiments, using VIL, echo top and lightning as predictors | 34 |
| B-2 | Summary of deviation prediction model experiments, using echo tops and lightning as predictors | 35 |
| B-3 | Summary of deivation predictin model experiments, using VIL and lightning as predictors | 37 |
| C-1 | Weather features contour boundaries used to define avoidance distances for deviating trajectories | 40 |

# 1. INTRODUCTION

Aviation weather systems such as the Corridor Integrated Weather System (CIWS) provide weather products and forecasts that aid enroute traffic managers in making tactical routing decisions in convective weather. However, enroute traffic managers need tools to aid them in the significant effort required to use the weather information to develop and execute a comprehensive plan to route traffic through the weather. Critical tasks – such as determining the impact of weather on existing traffic, devising a tactical response to mitigate the impacts of weather, predicting the effects of a particular routing strategy, predicting arrival times for flights traversing regions of convective weather – significantly increase controller workload and are often executed in a suboptimal manner due to the complexity of the tasks. Furthermore, different decision makers may reach very different conclusions about weather impact, because the subjective judgment of the decision maker is the primary 'tool' used to perform these tasks. A comprehensive decision support system that provides automated tools to integrate flight information, trajectory models and weather forecasts should help air traffic personnel make better and more pro-active decisions while reducing workload during convective events.

An important component in an integrated decision support system is the ability to predict when pilots in enroute airspace will choose to deviate around convective weather and how far they will deviate from their planned path. The FAA Aeronautical Information Manual suggests that pilots avoid thunderstorms characterized by "intense radar echo" in enroute airspace by at least 20 miles (32 km). However, a recent study (Rhoda, et al., 2002) suggests that pilots fly over high reflectivity cells in enroute airspace and penetrate lower reflectivity cells. Recent operational experience with CIWS in enroute airspace (Robinson, et al., 2004) supports the observations of (Rhoda, et al., 2002).

This study presents initial results of a study to develop a quantitative statistical model that predicts pilot deviation behavior in enroute airspace owing to convective weather. Data used in this study came from five different days in the summer of 2003 with significant convective weather in two different 'super-sectors' (regions defined by a small group of adjacent Air Traffic Control enroute sectors). An automated analysis process extracted enroute flight trajectories from the Enhanced Traffic Management System (ETMS) and calculated the planned trajectory corresponding to each actual flight trajectory extracted. A second automated analysis, the deviation detection algorithm, identified planned trajectories that encountered significant weather and determined if the aircraft significantly deviated from the planned trajectory. The results of the automated deviation detection algorithm were reviewed and edited by a human analyst. The edited deviation detection results and several statistical measures of the weather encountered along the planned trajectories (automatically extracted from CIWS weather data) provided the inputs to the deviation prediction model.

In addition to the deviation prediction model, this study presents an analysis of deviating flight trajectories and statistics that provide insight into deviation strategies. The avoidance distance (the distance from the boundary of the weather feature around which the pilot is deviating) was calculated for each deviating trajectory. The importance of deviation distance as a key factor in assessing ATC impact is illustrated graphically in the studies of "convectively constrained areas (CCAs)" that have been carried out in the context of validation of the Collaborative Convective Forecast Product (CCFP) (Mahoney, et al, 2004). The Figures in (Mahoney, et al., 2004) show that assuming aircraft will seek to stay at least 10 nmi away from any individual storm cell results in a very significant reduction in the usable airspace.

Finally, the study provides additional statistics about the weather that pilots actually encountered in enroute airspace. The study concludes with recommendations for follow on studies.

## 2. ANALYSIS METHODS

There were five steps in the deviation data analysis and model development:

1. Filter ETMS flight data to extract enroute flights and their actual and planned trajectories
2. Define operationally significant flight path deviation based on analysis of flight trajectories in clear weather
3. Calculate statistics that characterize weather encountered on planned and actual trajectories
4. Detect trajectory encounters with significant weather and weather-related deviations
5. Develop statistical model to predict deviations as a function of the input weather statistics

A flight was considered to be enroute through a super-sector (step 1) if its planned trajectory spent at least 15 minutes inside the super-sector boundaries and maintained an altitude greater than 25 kft for the complete trajectory. The planned trajectory was determined by applying the actual trajectory ground speed to the path defined by connecting the flight plan fixes from ETMS.

We defined deviation (step 2) as a flight trajectory whose mean *deviation distance* is greater than some deviation distance threshold. The deviation distance is the distance from each point on the planned trajectory to the nearest point on the actual trajectory. The *deviation threshold*, which represents the limits of normal operational variation in flight trajectories along the planned routes, was determined for each super-sector by an analysis of planned and actual trajectories on a single clear-air day: after trajectories with obvious short-cuts and re-routes were removed, the deviation threshold was defined as the 90$^{th}$ percentile of the mean deviation distance for the remaining trajectories.

Three CIWS products were used to characterize the weather (step 3):

1. Vertically Integrated Liquid (VIL): CIWS uses VIL as a measure of precipitation (see Robinson, et al., 2002 for a discussion of why VIL is preferred). VIL is mapped to an equivalent 6-level Video Integrator and Processor (VIP) scale of precipitation intensity (Troxel and Engholm, 1990). In this study, a higher resolution CIWS VIL product (the precursor to the 6 level display product) was used, so fractional VIP levels could be resolved.
2. High resolution radar echo tops: measure of storm cell height (Smalley et al., 1999)
3. Cloud-to-ground lightning strikes: measure of convective activity

For each trajectory (both planned and actual), weather statistics were calculated from two different sized neighborhoods, centered on the trajectory: 16km (approximating the clear-air route width) and 60km (approximating the 20 nm convective storm avoidance guidance given to pilots in the FAA Airman's Information Manual). Figure 1 illustrates the different route width scales.

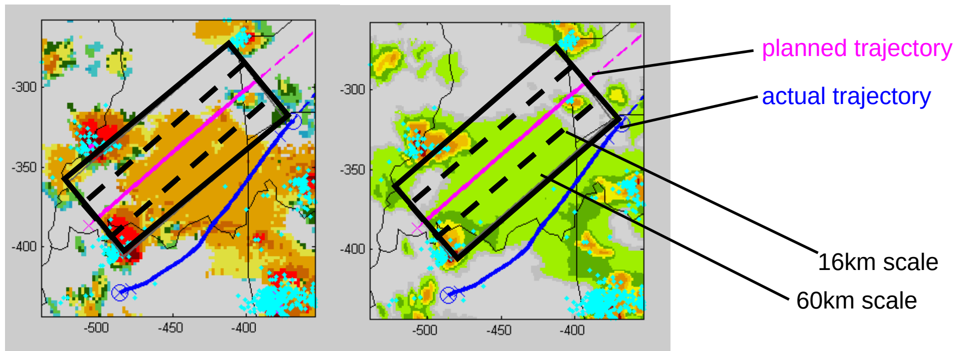


*Figure 1. Illustration of different neighborhood scales used in the extraction of weather data and calculation of weather statistics for weather encounters along planned and actual flight trajectories (example shows a planned trajectory neighborhood and weather encounter). Figure at left shows echo tops field, at right is VIL, cyan dots indicate cloud-to-ground lightning strikes. Solid line of each trajectory indicates the weather encounter.*

The weather statistics included mean, 90$^{th}$ percentile and maximum values for VIL, echo tops for and *deltaZ* (the difference between flight altitude and the echo top height, using different measures of echo top height) for both neighborhoods. For the 60km neighborhood, we calculated several additional statistics, including percentage of area covered by VIL levels >= level 3, 4 and 5; echo tops heights >= flight altitude, 30, 40 and 50 kft; and lightning counts in 6 minute time periods. A total of 31 statistical measures of weather characteristics were calculated. See Appendix A for a description of the complete set of weather statistics.

A weather encounter (step 4, Figure 1) was defined as the portion of a trajectory that passed through *either* VIL level 2 or greater *or* echo tops of 25 kft or greater for at least 2 minutes. The choice of VIL, echo top height and thresholds was based on a prior analysis of deviations around convective storms in enroute airspace (Rhoda, et al., 2002). Note that the weather encounter is not intended to be an *a priori* definition of convection or weather hazard. Rather, it is the definition of the *minimum* level of weather significant enough to be analyzed.

A planned trajectory weather encounter was flagged as a weather-related deviation if the mean deviation distance during the encounter was greater than the deviation threshold calculated in step 2. This set of automatically detected weather encounters and deviation flags were reviewed by an analyst and the deviation flags were edited when necessary.

The weather statistics and edited deviation flags from 595 weather encounters on 5 different summer days in 2003 provided the inputs to the deviation prediction model (step 5). Twenty different models were developed using the LNKnet pattern classification software developed at Lincoln Lab

(Lippmann, et al., 1993). In each model, a set of 5 weather statistics for each weather encounter (chosen from the complete set of 31) provided the inputs: two measures of VIL (one from the 16km neighborhood, the other from the 60km neighborhood), two measures of echo top height or *deltaZ*, and lightning counts from the 60km neighborhood. In order to test the assertion that both VIL and echo tops play a part in pilot decision, we developed twelve additional models with a set of 3 inputs: lightning and *either* echo tops *or* VIL from both neighborhood scales. In all models, we were careful to select sets of input variables that showed relatively low levels of cross-correlations. See Appendix B for a complete description of the weather model inputs.

We compared two different pattern classifiers: k-nearest neighbors, with several different values of k, and Gaussian. The Gaussian classifier proved to be the better of the two, and all models presented were based on Gaussian classifiers. In addition to predicting the output class (in this case, deviation or non-deviation), LNKnet also evaluates the explanatory power of each input variable by calculating the reduction in output classification error due to each input variable. A weather statistic that has high explanatory power in a deviation prediction model with a small output classification error is deemed to be an important factor in pilot decision.

In order to describe deviation strategies for the verified deviations, an analyst reviewed the actual trajectories flown and the weather encountered for 218 weather-related deviations. Each deviation was characterized by an *avoidance distance* from 24 different weather features (the minimum lateral distance between the deviating plane and the boundary of the weather feature that the pilot is avoiding). Weather features included VIL level 2, 3, 4 and 5 contours, echo top height of flight altitude, 30, 40 and 50 kft contours, and all VIL and echo top combinations. Avoidance distances were determined from a single *characteristic cross-section* chosen by the analyst to represent the weather encounter. The characteristic cross section is a line connecting the planned and actual trajectories that span the aviation hazard responsible for the deviation, in the analyst's judgment (see Figure 10 below). Statistics describing avoidance distances are presented.

## 3. RESULTS

### 3.1 CASE ANALYSIS

Flight trajectories in two 'super-sectors', ZID and ZOB, were analyzed. The ZID super-sector consisted of ATC sectors ZID66, ZID82 and ZID83; ZOB included ATC sectors ZOB28, ZOB46, ZOB48 and ZOB77. Figure 2 illustrates the super-sectors, showing the major enroute jetways and fair weather traffic in each. The majority of ZOB routes and traffic flow are carried along several parallel and closely spaced East-West oriented jetways. ZID traffic, by comparison, is evenly distributed among several jetways with different orientations. Demand, jetway orientations and spacing between jetways all impact the way in ATC manages flow and may constrain the deviation options in convective weather.

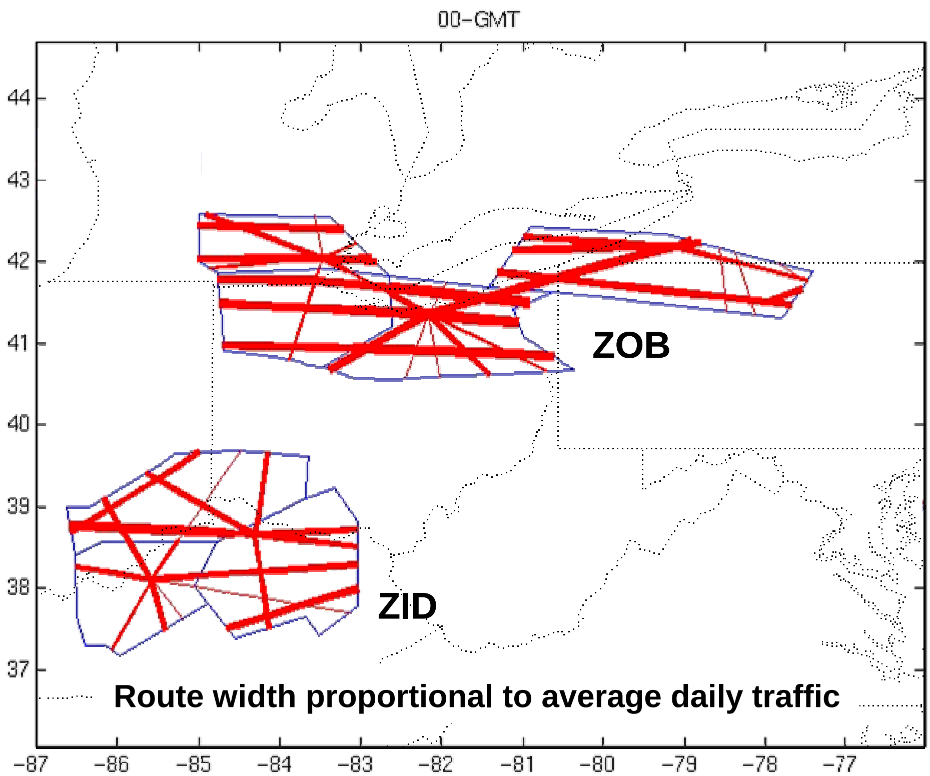


*Figure 2. Jetways and clear day traffic in super-sectors ZOB and ZID. Thickness of red lines indicates traffic load.*

A total of 472 enroute trajectories in ZID and 539 in ZOB during a clear 24-hour period (July 25, 2003) were analyzed to determine the deviation threshold. Figure 3 illustrates the deviation threshold analysis. It illustrates some examples of planned and actual trajectories extracted from the ETMS data. It also shows scatter plots of the mean deviation distance vs. the standard deviation of the deviation distance for each trajectory analyzed in each super-sector. A standard deviation threshold for each super-sector, selected by an analyst, was used to eliminate short cuts, reroutes and other intended deviations from deviation threshold analysis (vertical red lines in Figure 3). Trajectories whose mean deviation distance standard deviation was less than the threshold were assumed to be following the planned trajectory and the distribution of mean deviation distances among these trajectories represented the normal operational variation of pilots flying along their intended paths in the super-sector. The deviation threshold was selected as the 90$^{th}$ percentile of mean deviation distance of these 'normal' trajectories (horizontal magenta lines in Figure 3).

The deviation thresholds were 12 km for ZID and 24 km for ZOB. We found the difference in deviation thresholds between the two super-sectors somewhat surprising and cannot readily explain it using the available data.

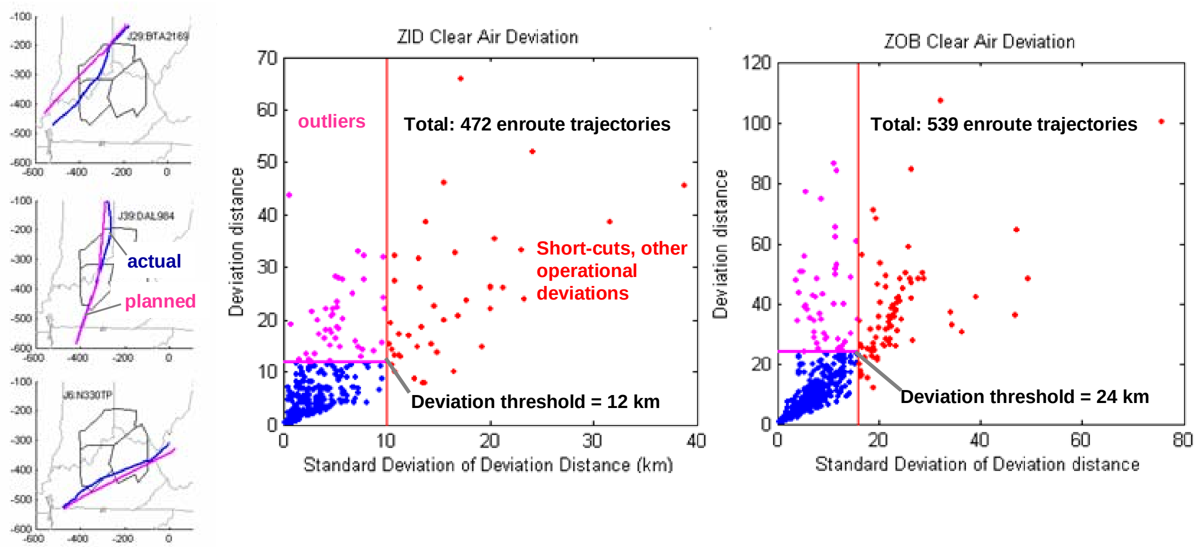


*Figure 3. Deviation threshold analysis in ZID and ZOB super-sectors. Column at left illustrates examples of planned and actual trajectories.*

Table 1 presents a summary of the case dates and times, the number of flights analyzed, the number of flights whose *planned* trajectories encountered significant weather, the total number of weather encounters detected and analyzed and the median and 90$^{th}$ percentile of VIL and echo tops measurements (based on the 16 km neighborhood) from the weather encounters. In general, convection in ZID was stronger, with echo tops and VIL levels significantly higher than what was observed in ZOB. Storm cells in ZID were also more clearly defined, with sharp boundaries between convective cells and areas of clear weather.

**TABLE 1**

**Summary of Weather Encounters for Planned Trajectories**

| Case start: finish | Sector | Trajectories | Trajectories with weather encounters | Weather encounters | VIL (median / $90^{th}$ pct.) | Echo tops (median/ $90^{th}$ pct.) |
|---|---|---|---|---|---|---|
| 2003/05/10 0500 : | ZID | 130 | 95 | 106 | 5.9 / 4.9 | 45 / 36 |
| 2003/05/10 1900 | **ZOB** | **168** | **62** | **69** | **4.5 / 2.9** | **33 / 26** |
| 2003/06/14 1500 : | ZID | 134 | 67 | 66 | 5.6 / 5.0 | 37 / 31 |
| 2003/06/15 0000 | **ZOB** | **279** | **24** | **21** | **4.9 / 4.6** | **31 / 28** |
| 2003/06/26 2000 : | ZID | 142 | 120 | 128 | 4.9 / 4.0 | 30 / 38 |
| 2003/06/27 0500 | **ZOB** | **220** | **151** | **122** | **4.5 / 3.4** | **29 / 24** |
| 2003/07/09 1600 : | ZID | 219 | 168 | 220 | 5.8 / 4.8 | 46 / 37 |
| 2003/07/10 1300 | **ZOB** | **531** | **41** | **36** | **4.5 / 2.8** | **33 / 26** |
| 2003/07/31 0800 : | ZID | 74 | 52 | 75 | 5.0 / 3.9 | 32 / 27 |
| 2003/07/31 1800 | **ZOB** | **223** | **1** | **0** | **N/A** | **N/A** |
| **Totals (ZID/ZOB/both)** | | **699/1421/2120** | **502/279/781** | **595/248/843** | | |

Figures 4 and 5 illustrate typical storm deviations identified by the automatic detection algorithm. The panels at the left of the figures show weather fields (VIL on top, echo tops on bottom) with planned (magenta line) and actual (blue line) trajectories over laid. Solid portions of the trajectories indicate the weather encounter identified by the algorithm. The panels at right show the VIL (top) and echo tops (bottom) that the flight would have encountered (magenta plot) and actually encountered (blue plot) along its trajectory.

In these examples, convective storm cells are characterized by high VIL, echo tops well above the flight level and lightning activity. Cell complex boundaries are readily evident, and flight trajectories clearly deviate around vigorous convective activity. Many weather encounters and deviations in the ZID super-sector exhibited similar characteristics.

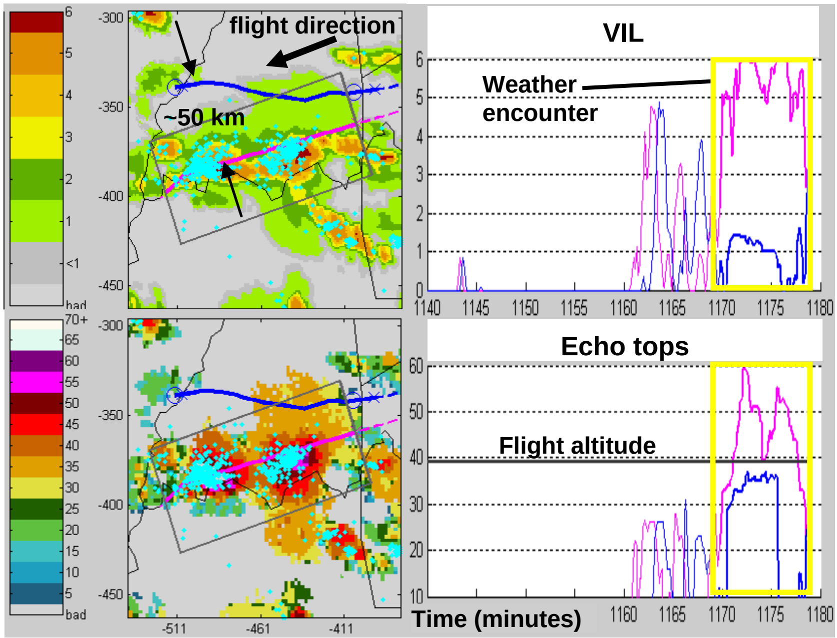


*Figure 4. A typical storm cell deviation in the ZID super-sector.*

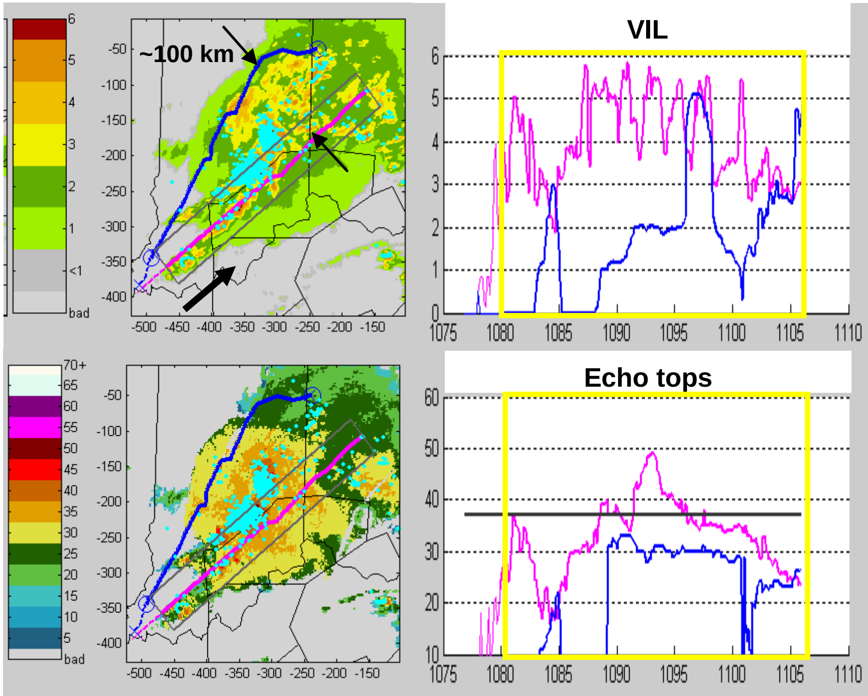


*Figure 5. A typical storm cell deviation in the ZID super-sector.*

Weather encounters in ZOB were not so easily characterized. In the five cases studied, the weather was largely stratiform precipitation with embedded weak convective cells. Flight path deviations were also less predictable, which might be expected given the wider distribution of clear air deviation distances. Figures 6 and 7 illustrate examples.

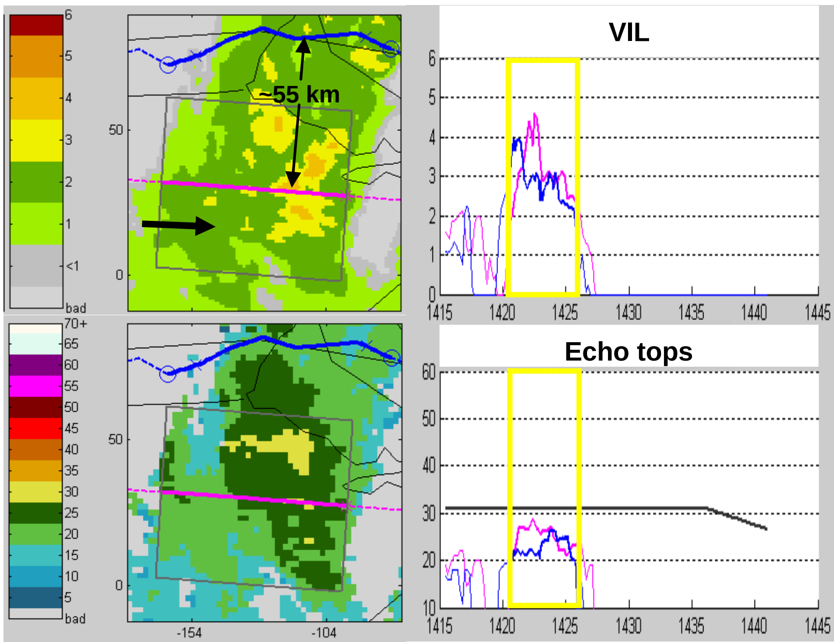


*Figure 6. A typical weather-related deviation in the ZOB super-sector.*

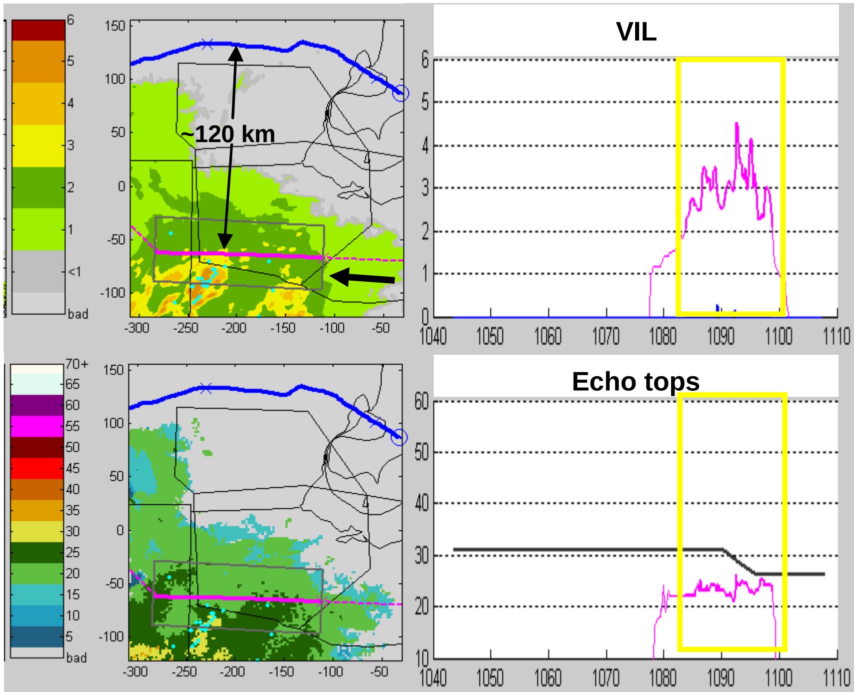


*Figure 7. A typical weather-related deviation in the ZOB super-sector.*

The automated deviation detection algorithm classified planned trajectory weather encounters as weather-related deviations or non-deviations, using the methods, definitions and thresholds described above in section 2. The results of the automated deviation detection algorithm were reviewed by an analyst, who inspected every weather encounter (both deviations and non-deviations) that was identified and classified by the detection algorithm. The analyst reviewed planned and actual trajectories and VIL, echo tops and lightning strike maps in the vicinity of the weather encounter to determine if the detection algorithm was correct.

The automated algorithm detected and classified 595 weather encounters in ZID and 248 in ZOB. The analyst was able to verify the deviation flag for 490 of the encounters in ZID and 176 in ZOB. The probability of detection and false alarm rate was calculated for the automated deviation detection algorithm using the verified encounters. The performance of the deviation detection algorithm is summarized in Table 2.

**TABLE 2**

**Summary of Automated Deviation Detection Algorithm Performance**

| Case | Sector | Deviations POD / FAR | Non-deviations POD / FAR |
|---|---|---|---|
| 2003/05/10 | ZID | 93.9 / 7.5 | 80.0 / 16.7 |
| | **ZOB** | **90.0 / 30.8** | **92.7 / 1.9** |
| 2003/06/14 | ZID | 86.7 / 10.3 | 90.9 / 11.8 |
| | **ZOB** | **NA / 100.0** | **80.0 / 0.0** |
| 2003/06/26 | ZID | 69.6 / 38.5 | 88.6 / 8.2 |
| | **ZOB** | **71.4 / 48.3** | **86.1 / 6.5** |
| 2003/07/09 | ZID | 94.9 / 3.7 | 90.2 / 13.2 |
| | **ZOB** | **100.0 / 40.0** | **81.0 / 0.0** |
| 2003/07/31 | ZID | 87.5 / 33.3 | 86.0 / 4.4 |
| | **ZOB** | **NA / NA** | **NA / NA** |
| All cases | ZID | 91.2 / 10.8 | 87.9 / 10.0 |
| | **ZOB** | **81.1 / 44.4** | **87.2 / 4.1** |

Deviation detection error rates were significantly higher in ZOB than in ZID. Several factors may have contributed to the difference in performance: clear air routes appeared to be flown much tighter in ZID[1], making the difference between deviation and non-deviation more obvious; convective cells in ZID were stronger and more clearly defined in ZID than in ZOB; ATC may employ different weather avoidance strategies in the two super-sectors. Further study is required to establish a better definition of operationally significant deviation, a clear description of the failure modes of the deviation detection algorithm and to devise improvements to address them.

### 3.2 DEVIATION PREDICTION MODEL

Inputs to the deviation prediction model consisted of 490 planned trajectory weather encounters from super-sector ZID whose classification (deviation or non-deviation) could be verified by the analyst. ZOB weather encounters were not considered because of the difficulty in detecting and identifying weather-related deviations, the relatively small number of encounters that deviated (32 of 176, or 18%) and the significant difference between the two super-sectors in weather characteristics and clear-air deviation thresholds.

[1] This difference seems counter intuitive given the respective route structures in ZOB and ZID.

Several general trends appeared in the results of the modeling experiments:

1. Overall prediction errors (combined deviation and non-deviation) ranged from 19% to 26%. However, models differed significantly in the differences between deviation and non-deviation prediction errors (ranging from 2% to 28%). The better models were characterized by both low overall prediction errors and a small difference between the deviation and non-deviation prediction errors.

2. In 19 of the 20 modeling experiments that included both VIL and echo top measurements as inputs, the most powerful explanatory input was a measure of echo top height.

3. In the 11 modeling experiments with the lowest overall classification error rate, the most powerful explanatory input was a measure of *deltaZ* (flight altitude – echo top height), based on a 90$^{th}$ percentile measure of echo top height within the analysis neighborhood (either 16km or 60km). The second explanatory input was a measure of VIL.

4. Models that used 90$^{th}$ percentile weather measurements as inputs yielded results at least as good as or better than average measurements in all cases.

5. Lightning appears to add little value as a predictor when both echo top height and VIL measures are available.

These general trends indicate that the primary factor in weather-related deviations is the height of the storm relative to the flight altitude, with VIL or precipitation measurements reducing the difference in prediction errors for deviation and non-deviation, in some cases. Furthermore, spatial averaging of weather data measurements (either echo top height or VIL) appears to reduce the explanatory power of the data.

The results from the twelve additional models, in which lightning and only VIL or echo top measurements provided the weather inputs, were consistent with these findings. Error rates for the echo top-only models were lower than those from VIL-only models.

Modeling results for all 32 models are summarized in Figure 8. The blue boxes show the overall error in predicting both deviations and non-deviations, the red show the error in predicting deviations, the green show the error in predicting non-deviations for a given model.

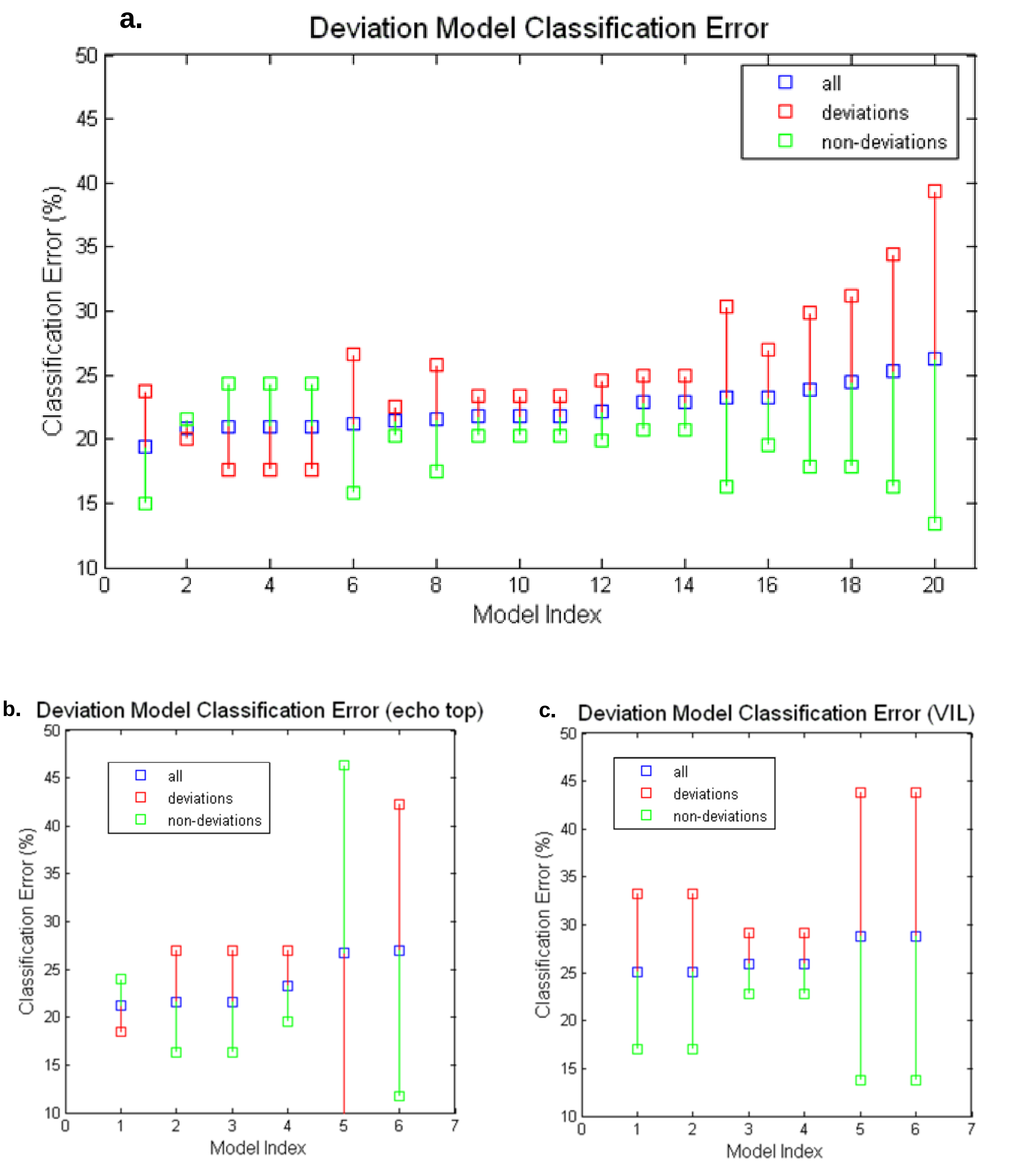


*Figure 8. Summary of deviation prediction model errors. Figure (a) shows results for models with VIL, echo top height and lightning inputs, (b) shows results for echo top and lightning inputs, (c) for VIL and lightning inputs. Appendix B describes the predictors that correspond to each model index (x-axes).*

Figures 9 - 11 provide a more detailed look at the prediction model inputs and results for one of the models (model index 9, from Figure 8a). Figure 9 shows four 2D histograms: deviation counts, non-deviation counts, observed probability of deviation (percentage of flights in each histogram bin that deviated) and a smoothed probability density function derived from the statistics. The histograms axes are the two best predictors of deviation according the to the deviation model: the percentage of the pixels in the 60 km neighborhood whose VIL is level 3 or greater (x axis) and deltaZ, using the 90$^{th}$ percentile echo top height from the 16 km neighborhood (y axis).

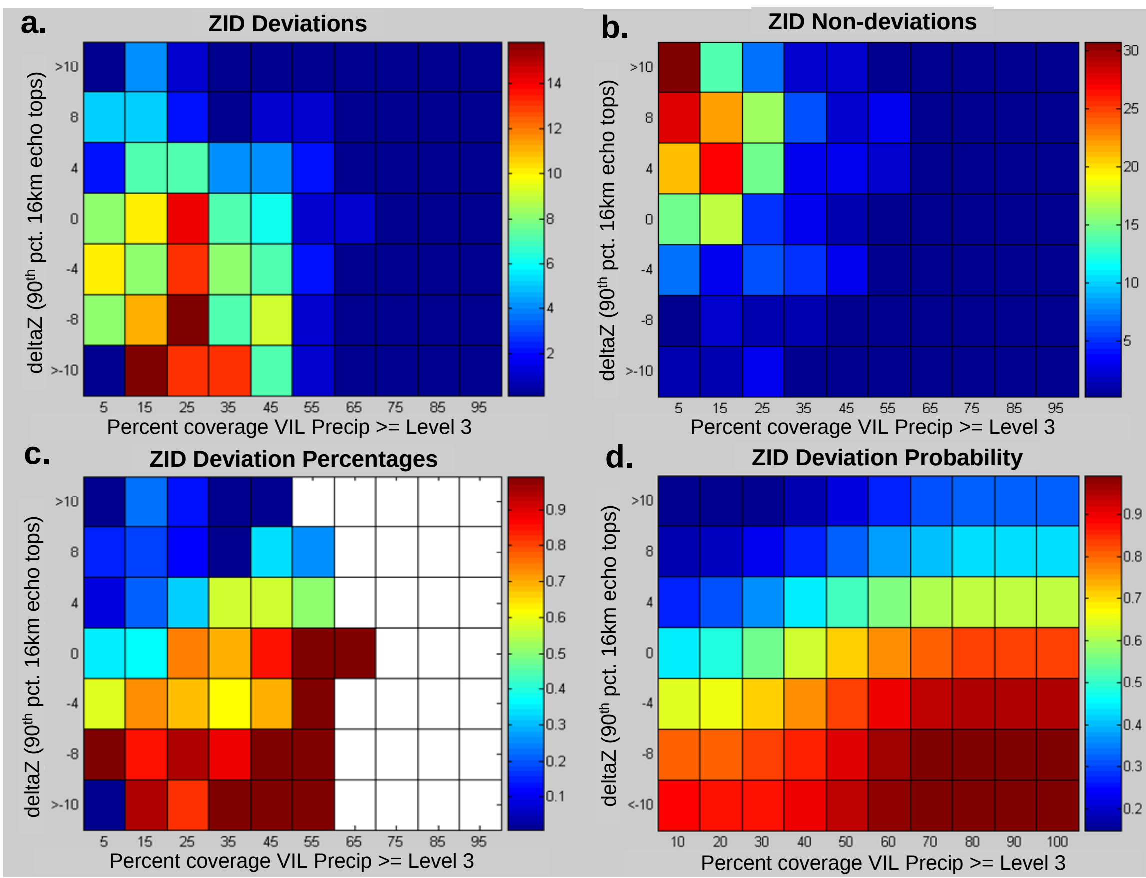


*Figure 9. 2D histograms of deviation counts (a), non-deviation counts (b), observed probability of deviation (percentage of flights in each histogram bin that deviated) (c) and a smoothed probability function derived from the observed probabilities (d).*

Figure 10 shows the relationship between the weather inputs and the result (deviation or not). Figure 10a is a table that ranks the inputs in order of their predictive power, and the cumulative output classification error as each input is added to the model. In this model, the addition of the third, fourth or fifth inputs (percentage of pixels in the 60 km neighborhood with echo tops >= 40kft, 90th percentile VIL level in the 16 km neighborhood and lightning counts) resulted in a small increase in classification error. Figures 10b and 10c show four histogram plots. The upper plots show the distribution of the deltaZ and VIL level 3 percentage measurements, partitioned into deviations and non-deviations. If the deviations and non-deviations are well separated, the input will be a good predictor of deviation; if there is considerable overlap, it will not. The bottom histogram is the distribution of correct and incorrect classifications of deviation and non-deviations. Correct classifications are above the x axis, incorrect ones are below. Note that the majority of classification errors occur for trajectories whose weather characteristics fall in the interval where deviations and non-deviations overlap.

**a.**

**Cumulative Classification Error**

| | |
|---|---|
| **deltaZ** | **24.49** |
| **% VIL >= level 3** | **21.22** |
| % echo top >= 40 kft | 21.43 |
| VIL 90th percentile | 22.04 |
| Lightning | 21.84 |

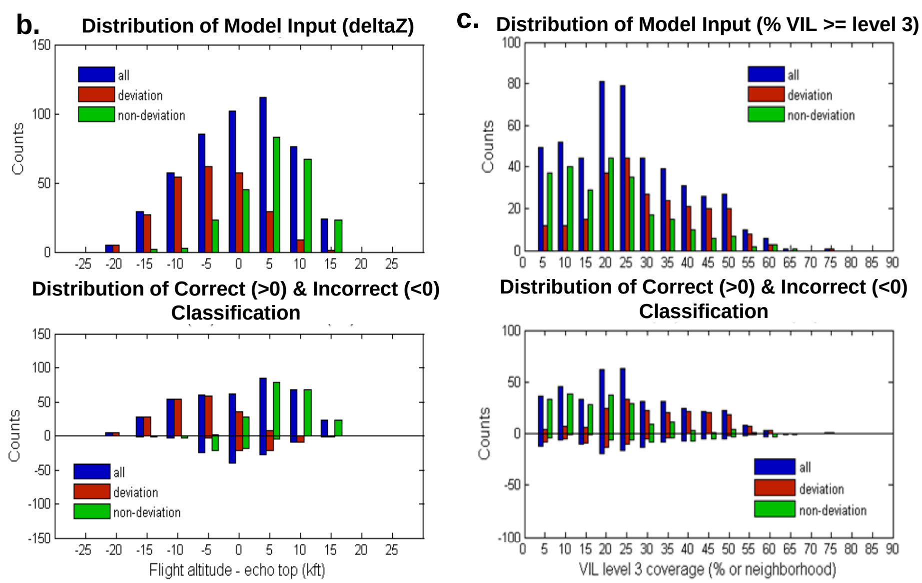


*Figure 10. Relationship between weather inputs and deviation / non-deviation result. Table **(a)** ranks the weather inputs in order of explanatory power, with the cumulative deviation prediction error. Histogram **(b)** shows distribution of deltaZ for all weather encounters (blue), deviations (red) and non-deviations (green). Histogram **(c)** shows the same for VIL level 3 percent coverage.*

Figure 11 is a scattergram of the two best predictor values (VIL level 3 percentage on the x axis, deltaZ on the y axis) for each weather encounter plotted on top of the decision half-planes (deviation in gold and non-deviation in red) determined by the deviation prediction model. The deviation prediction for an input data point (i.e., a planned trajectory weather encounter) is determined by the decision region in which it falls. Decision region boundaries may be suspect in regions where data is sparse – a model performs best where there is sufficient data!

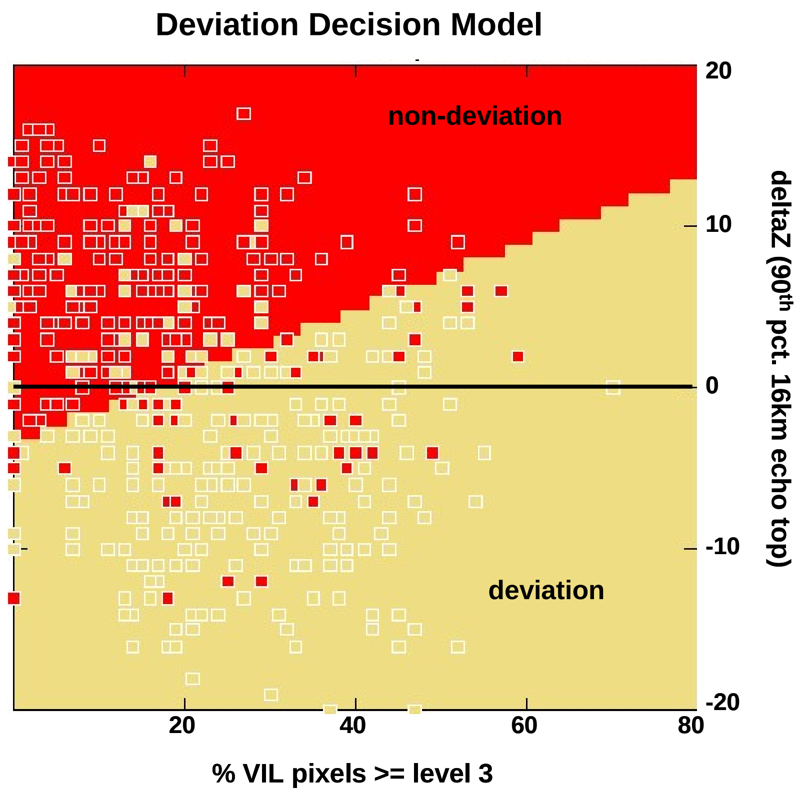


*Figure 11. Deviation decision plot, as a function of weather input variables. X axis is percent of VIL pixels in the 60 km route region that are level 3 or greater. Y axis is deltaZ, (flight altitude – 90th percentile echo top height from the 16 km route region).*

Finally, Figure 12 shows the histograms of lightning counts for all weather encounters, partitioned into deviations and non-deviations, for both ZID and ZOB. It is evident from the histograms that lightning counts in the 60 km neighborhood may provide some predictive skill, if data such as echo tops or VIL are not available.

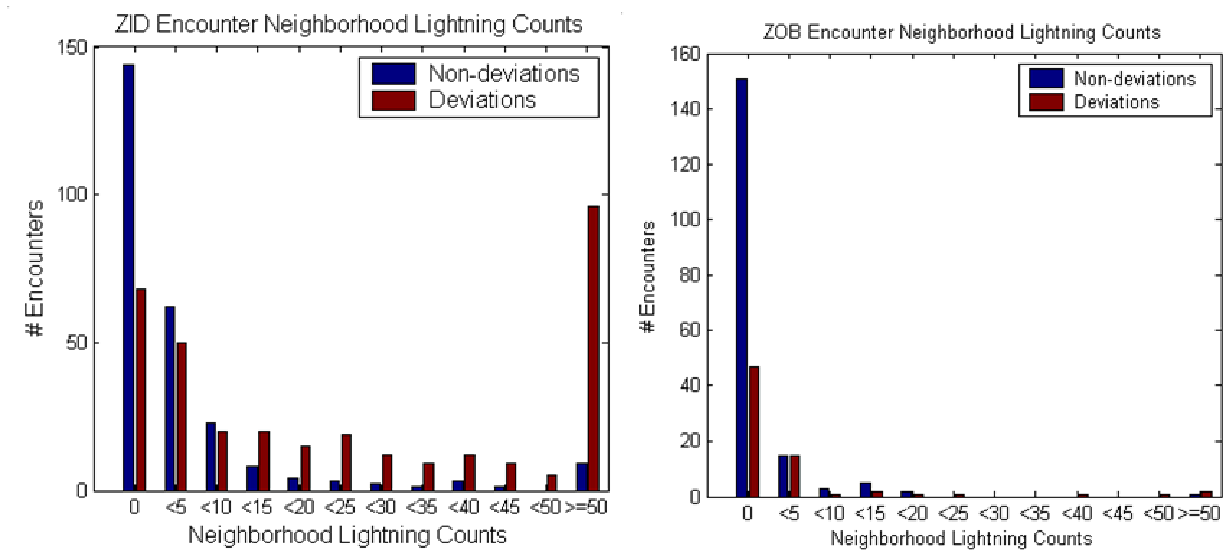


*Figure 12. Histograms of lightning counts within the 60km encounter neighborhood box in the 6 minutes immediately prior to weather encounters in ZID and ZOB.*

### 3.3 AVOIDANCE DISTANCE ANALYSIS

Avoidance distances were determined from a single characteristic cross-section specified by the analyst for each deviation. A second analyst reviewed the cross-sections, but the choice of a single cross-section to characterize the deviation strategy is somewhat subjective. In some instances, the analyst could not make a sensible choice of cross-section. Of the 248 verified deviations in ZID, cross-sections were selected from 220. Appendix C describes in detail the process used to determine weather feature boundaries and presents the full set of avoidance statistics.

The data automatically extracted from the VIL and echo top fields along the cross-section define *avoidance distance curves,* which show VIL and echo top height as a function of position along the cross section. Using the point of intersection between the cross-section and the actual trajectory, the avoidance distance from different weather feature boundaries may be calculated automatically from the avoidance distance curve. Figure 13 illustrates an example.

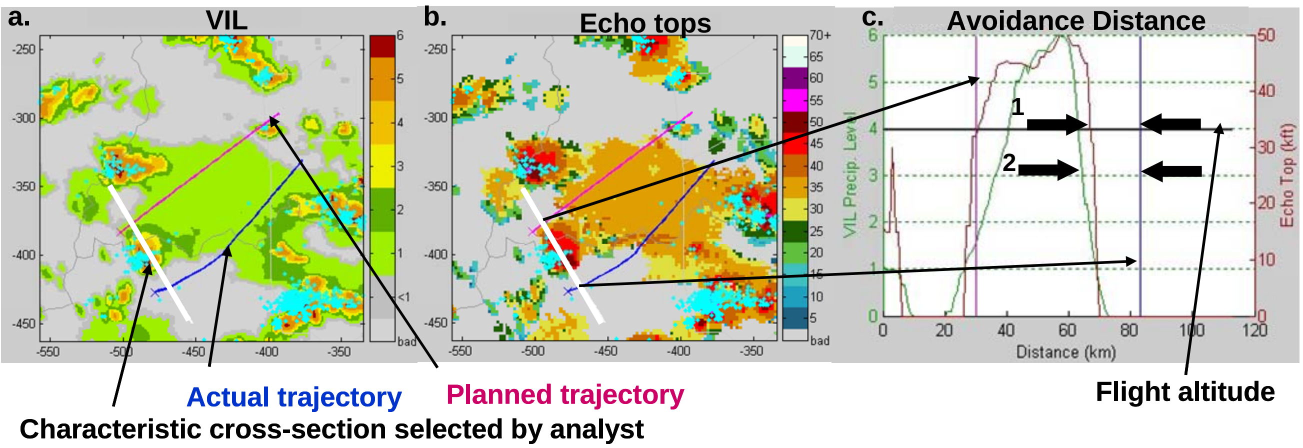


*Figure 13. Avoidance distance analysis. Figure **(a)** shows the **planned** and **actual** trajectories from a deviation overlaid on the VIL field; figure **(b)** shows the echo top field; figure **(c)** shows the avoidance distance curves for VIL and echo tops along the characteristic cross-section. Arrows labeled **(1)** show the avoidance distance for echo top height equal to flight altitude, arrows **(2)** show avoidance of VIL level 3.*

Unfortunately, not all deviation strategies and avoidance distance determinations were as clear-cut as those illustrated in Figure 13. Figure 14 illustrates an example where neither the hazard nor the deviation strategy is clear.

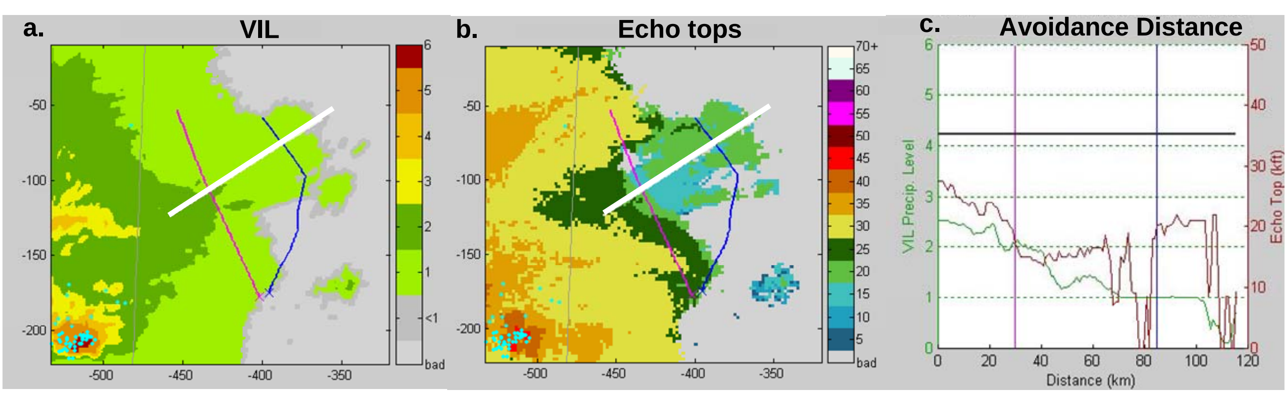


*Figure 14. Illustration of an unclear deviation strategy. Pilot makes a large deviation in a region of benign weather, more than 100 km downwind from nearest convective cell.*

Of all 24 avoidance distances calculated, those for VIL level 2, 3 and 4 features were the most consistent, implying that VIL level contours may provide the best hazard boundary for deviating pilots. Approximately 75% of all deviating aircraft (168 of 218) flew within 20 km of the VIL level 2 boundary, within 25 km of the VIL level 3 boundary and within 33 km of the VIL level 4 boundary. This suggests a two step process to create a ‘convective hazard field’: (1) use flight altitude, echo tops and VIL to find hazardous cells, (2) find the VIL level contours that bound the hazardous cells.

It is important to note that one must use caution in interpreting the avoidance analysis data. Given the small data set analyzed, it is impossible to make a definitive statement about avoidance distances and deviation strategies used by pilots to avoid convective weather. Moreover, deviation strategies are not easily inferred from weather and trajectory data due to the complexity of convective weather and traffic patterns in busy airspace, the lack of concrete evidence about what information sources are used by the pilot and the fact that the deviation strategy may be imperfectly executed and therefore, the actual trajectory flown may not reflect the pilot’s intent. More research is necessary to understand the specific relationships between weather, traffic and deviation strategies.

### 3.4 WEATHER PENETRATION

Figure 15 summaries the penetrations in the ZID super-sector for all case days; Figure 16 does the same for ZOB. The figures indicate that while most of the ‘penetrations’ are actually over-flights, a significant percentage of pilots are willing to penetrate regions of high echo tops and VIL that would be characterized as a high avoidance region by the deviation prediction model. These results suggest VIL and echo top height alone are not sufficient to define completely convective regions that pilots wish to avoid. Other weather factors (e.g., storm growth or decay, direction of storm motion, etc.) or weather characteristics that the pilot sees (e.g., the presence or absence of thunderstorm turrets, radar reflectivity as sampled by the aircraft weather radar, etc.) are likely to play a part in pilot decision making. It is also possible that there is a significant range in pilots’ risk tolerance.

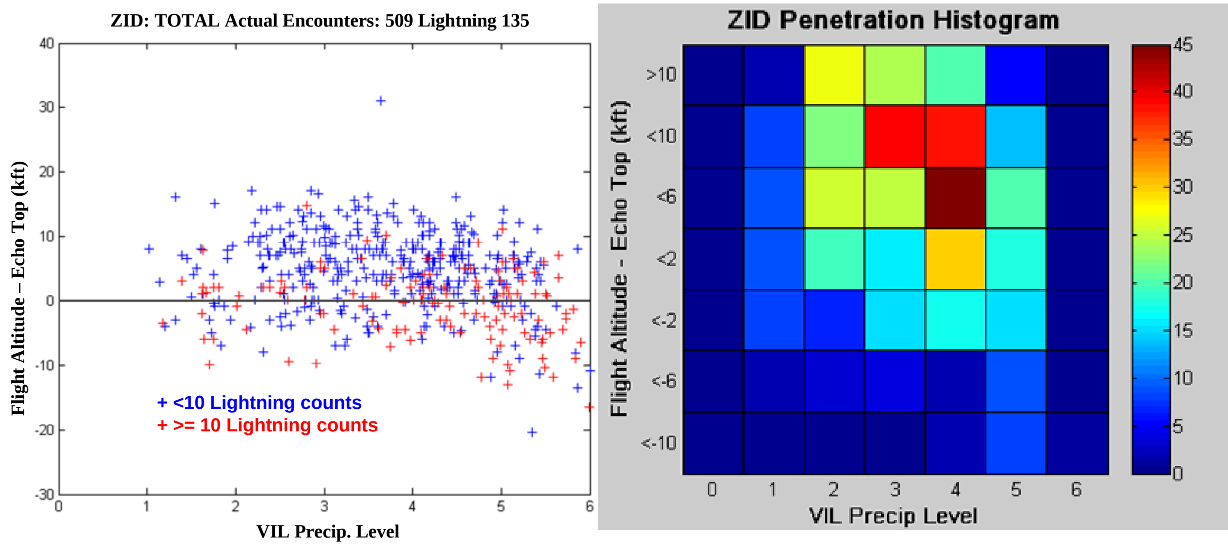


*Figure 15. ZID penetrations. Scattergram at left shows plots deltaZ vs. VIL level for all actual trajectory weather encounters. Blue + indicate encounters where the neighborhood cloud to ground lightning count was <10; red + indicates counts >=10. Data points above the 0-line represent over-flights, where flight altitude > echo top height. Plot at right is the histogram of the weather encounter data.*

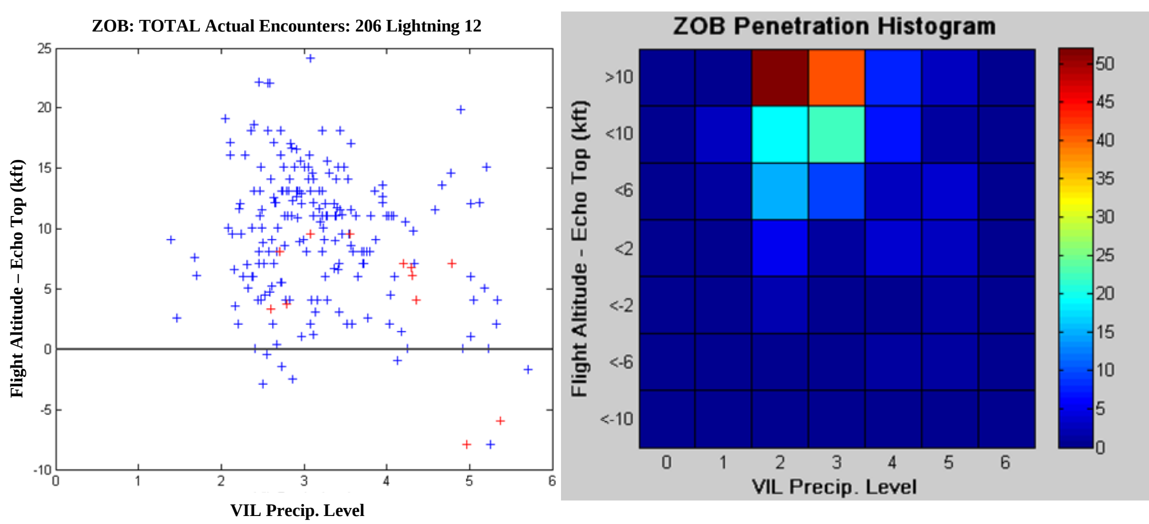


*Figure 16. ZOB penetrations. Plots as in Figure 15.*

# 4. SUMMARY, CONCLUSIONS AND ADDITIONAL WORK

This study presents initial results of a model to predict enroute flight deviations due to convective storms. The model was developed by applying statistical pattern recognition techniques to:

- high resolution VIL and echo tops data from CIWS and cloud-to-ground lightning strike counts from NLDN to characterize the weather, and

- flight plan and trajectory data from ETMS to determine planned and actual enroute flight trajectories and deviations.

A method for determining the bounds of convective regions that deviating pilots wish to avoid and a statistical distribution of avoidance distances were presented. Statistics describing the penetration and overflight of convective weather were also presented. Weather and flight data from over 800 different trajectories on five different days in two different air traffic control ‘super-sectors’ (ZID and ZOB) were analyzed.

A deviation prediction model could be developed only in the ZID super-sector, where the convective cells were generally strong and well-defined. A sufficient number of verified deviating and non-deviating flight trajectories were found and the difference between deviating and non-deviating flight trajectories was clear. The results of the modeling experiments were clear and consistent:

1. Deviation prediction models with error rates for both deviations and non-deviations below 25% were possible, using several different sets weather data measurements as inputs.

2. In all modeling experiments (except those with VIL only), *deltaZ* (the difference between flight altitude and echo top height) was the most powerful predictor of deviation. The use of 90$^{th}$ percentile echo top measurements in the calculation of deltaZ resulted in lower errors than average values of echo top height.

3. Measurements of VIL, without echo top heights, proved to be relatively poor predictors of deviation, when compared to models with echo tops only or both echo tops and VIL. However, the combination of echo tops and VIL measurements in the input data set reduced the spread between errors in predicting deviations and non-deviations from that achieved by using echo tops and lightning alone.

For all verified deviations, avoidance distances from 24 different weather features were calculated, where possible, based on input from an analyst. Avoidance distances for 220 deviations were analyzed. Seventy-five percent of deviating trajectories passed within 20 km of the VIL level 2 boundary, within 25 km of the level 3 and within 33 km of the level 4 boundary. This suggests that a model for deviation strategy may use echo tops and VIL together to predict where planned trajectories will encounter regions of weather that the pilot will wish to avoid, and best define the deviation distance.

Weather penetration statistics were also gathered for more than 700 weather encounters in both ZID and ZOB super-sectors. The data suggest that pilots are willing to fly over level 4 and even level 5 VIL if they can clear the echo tops by 4 - 6 kft, and that a significant percentage of pilots will penetrate regions of high echo top and VIL that would be determined to be likely avoidance regions by the deviation prediction model. This indicates that VIL and echo tops alone are not sufficient to define regions of convective weather that pilots will seek to avoid and / or that there is a significant range in pilot risk tolerance.

Finally, it must be noted that this is an ***exploratory*** **study.** The conclusions were limited by the small size of the input data set and the immaturity of the algorithms used to analyze trajectories and characterize weather encounters. We clearly need to examine many more convective weather cases in a number of different regions. For example, it is very important to determine if there are differences in pilot behavior in highly congested airspace where there are closely spaced routes going roughly in the same direction (e.g., ZOB , ZNY and possibly ZDC) versus ARTCCs where there is much greater distances between the routes (e.g. ZME) or where there are significant crossing traffic flows (e.g. ZID). ARTCCs that are principally transitional airspace (e.g., ZAU, ZTL, and ZFW) may also have significantly different pilot behavior.

Several additional studies could provide key information that could improve deviation modeling:

**1) Improved definition and detection of deviation.** More work is needed to develop a better operational definition of deviation that considers factors not accounted for in this study, including sector route structure, prevalent ATC routing strategies and characteristics of convective weather.

**2) Addition of other relevant weather data.** Upper-level winds from RUC and storm motion vectors from CIWS provide information necessary to determine if a planned or actual trajectory is downwind or upwind of a convective cell, or in front of or behind the path of a moving storm. Information about cell growth and decay is also likely to be important. Operational evidence suggests that pilots may be more willing to penetrate regions with higher VIP levels on the trailing edge of a storm where cells are decaying, while avoiding lower VIP levels on the leading edge where cells are actively growing (DeLaura and Allan, 2003). PIREPs are also likely to affect pilot decisions in convective weather.

Another important weather feature may be the nature of the convective weather. Having an accurate model to predict whether pilots will fly through gaps in squall lines is very important operationally as is the deviation distance around the ends of squall lines. It is also important to determine if there are differences in the pilot behavior with air mass thunderstorms versus other types of “disorganized” convection.

**3) Improved hazard avoidance distance calculation algorithms.** The hazard avoidance distance calculation used in this study is compact and easily analyzed. However, it was labor intensive, provided only a small sampling of the available data and could not be applied to approximately 15% of all verified deviations, where complicated weather patterns resulted in deviation strategies that could not be characterized by a single avoidance distance.

**4) Inclusion of more factors in prediction of deviation strategies.** Deviation strategies most likely involve several factors not considered here: availability of clear airspace nearby, airspace constraints due to sector route geometry or traffic, etc.

# APPENDIX A
# WEATHER STATISTICS USED TO CHARACTERIZE CONVECTIVE WEATHER

Three products were used to characterize the weather encountered by planned and actual flight trajectories in this study: Vertically Integrated Liquid (VIL), radar echo tops (18 dBZ reflectivity) and cloud-to-ground lightning strikes. VIL provides a measure of precipitation intensity, echo tops provide an estimate of the height of the storm and lightning generally indicates the presence of strong updrafts associated with convection. In CIWS, VIL is calculated from NEXRAD reflectivity data. VIL, which is defined as mass per unit area (e.g. $kg/m^2$), is mapped to an equivalent radar reflectivity (dBZ) scale, which is, in turn, mapped to the 6-level Video Integrator and Processor (VIP) scale of precipitation intensity (Troxel and Engholm, 1990). The seven points on the VIP scale (the zero point and the 6 VIP levels) are assigned values on the CIWS VIL interest level scale, which ranges from 0 to 255 (see table A-1). A piecewise inverse log function was used to interpolate intermediate VIL values to CIWS VIL interest level.

**TABLE A-1**

**VIL to Interest Level Mapping**

| VIL ($kg/m^2$) | Reflectivity (dBZ) | VIP Level | CIWS VIL Interest Level |
|---|---|---|---|
| 0.05 | <18 | 0 | 0 |
| 0.14 | 18 | 1 | 42 |
| 0.7 | 30 | 2 | 84 |
| 3.5 | 41 | 3 | 128 |
| 6.9 | 46 | 4 | 170 |
| 12.0 | 50 | 5 | 212 |
| 32.0 | 57 | 6 | 255 |

We examined 31 different statistical measures of these products on two different spatial scales (16 km and 60 km route widths) in an effort to determine which weather characteristics were most important in the pilots' deviation decision. Table A2 lists the statistics.

## TABLE A-2

### Weather Statistics Used to Characterize Weather Encounters along Planned and Actual Flight Trajectories

| Statistic | 16 km name | 60 km name | Comments |
|---|---|---|---|
| Maximum VIL | vilmax_16 | vilmax_60 | |
| $90^{th}$ percentile VIL | vil90_16 | vil90_60 | $90^{th}$ percentile used as lower noise surrogate for max. value |
| Average VIL (>= level 3) | vil3avg_16 | vil3avg_60 | Average of all VIL pixels >= VIL level 3 encountered along trajectory |
| VIL 'pain' | vilpain_16 | | Time integral of VIL pixels >= VIL level 3 encountered along trajectory |
| Average VIL | | vilavg_60 | Average of all VIL pixels encountered along trajectory |
| VIL standard deviation (>= level 3) | | vil3std_60 | Standard deviation about mean of all VIL pixels >= level 3 |
| VIL standard deviation | | vilstd_60 | Standard deviation about mean of all VIL pixels |
| % VIL pixels >= level 3 | | l3pct_60 | |
| % VIL pixels >= level 4 | | l4pct_60 | |
| % VIL pixels >= level 5 | | l5pct_60 | |
| Maximum echo top | etmax_16 | etmax_60 | |
| $90^{th}$ percentile echo top | et90_16 | et90_60 | $90^{th}$ percentile used as lower noise surrogate for max. value |
| Average echo top (>=30 kft) | et30avg_16 | et30avg_60 | Average of all echo top pixels >= 30 kft encountered along trajectory |
| Echo top 'pain' | etpain_16 | | Time integral of echo top pixels >= 30 kft encountered along trajectory |
| Average echo top | | etavg_60 | Average of all echo top pixels encountered along trajectory |
| Echo top standard deviation (>= 30 kft) | | et30std_60 | Standard deviation about mean of all echo top pixels >= 30 kft |
| Echo top standard deviation | | etstd_60 | Standard deviation about mean of all echo top pixels |
| % echo top pixels >= 30 kft | | et30pct_60 | |
| % echo top pixels >= 40 kft | | et40pct_60 | |
| % echo top pixels >= 50 kft | | et50pct_60 | |
| *deltaZ* using echo top max | dzetmax_16 | dzetmax_60 | *deltaZ* calculated using maximum value of echo top encountered along trajectory |
| *deltaZ* using $90^{th}$ percentile echo top | dzet90_16 | dzet90_60 | *deltaZ* calculated using $90^{th}$ percentile value of echo top encountered along trajectory |
| Lightning | | lght_60 | Six-minute count of cloud-to-ground lightning strikes |

It is important to note that VIL, echo tops and cloud-to-ground lightning by themselves are not sufficient to identify regions of intense convective activity and potential convective hazards with complete accuracy. For instance, high VIL and high echo tops may be present in decaying storm cells that pilots appear willing to penetrate. In these cases, the VIL is concentrated at lower altitudes in the collapsed storm core, but sufficient liquid remains aloft to result in high (but relatively benign) echo tops. Better measures of vertical reflectivity structure (e.g. reflectivity at higher altitudes, echo tops based on different reflectivity values, etc.) provide additional information about the weather that may help to better identify regions of vigorous convection.

The use of cloud-to-ground lightning is also less than ideal; cloud-to-ground lightning is often associated with decaying convection (Williams et al., 1989; Cary and Rutledge, 1996). Intracloud lightning is more often associated with growing, vigorous convection, but data is more difficult to collect.

# APPENDIX B
# DEVIATION MODELING

The data set used in the deviation prediction modeling consisted of 490 flights from the ZID super-sector whose planned trajectories encountered significant weather. Flights whose mean deviations (mean distance between the planned and actual trajectories) exceeded the deviation threshold were classified as deviations; flights whose mean deviation was less than or equal to the deviation threshold were classified as non-deviations. Several modeling experiments were run to determine which weather characteristics best predicted deviation. Each experiment used a different subset of the input weather statistics described in Appendix A as deviation predictors.

In building each prediction model, several subsets of the 490 flights were randomly selected for use as the model training data set. Flights in the training data set were partitioned in deviations and non-deviations, and the distribution of the input predictor values for both deviations and non-deviations were approximated by Gaussians. The ability of a predictor to discriminate between deviations and non-deviations is related to the degree of overlap between the two distributions; where the two distributions overlap, there is considerable uncertainty in predicting the result (see Figure B1). When multiple predictors are used, it is important that they be as uncorrelated as possible, since highly correlated predictors provide redundant information.

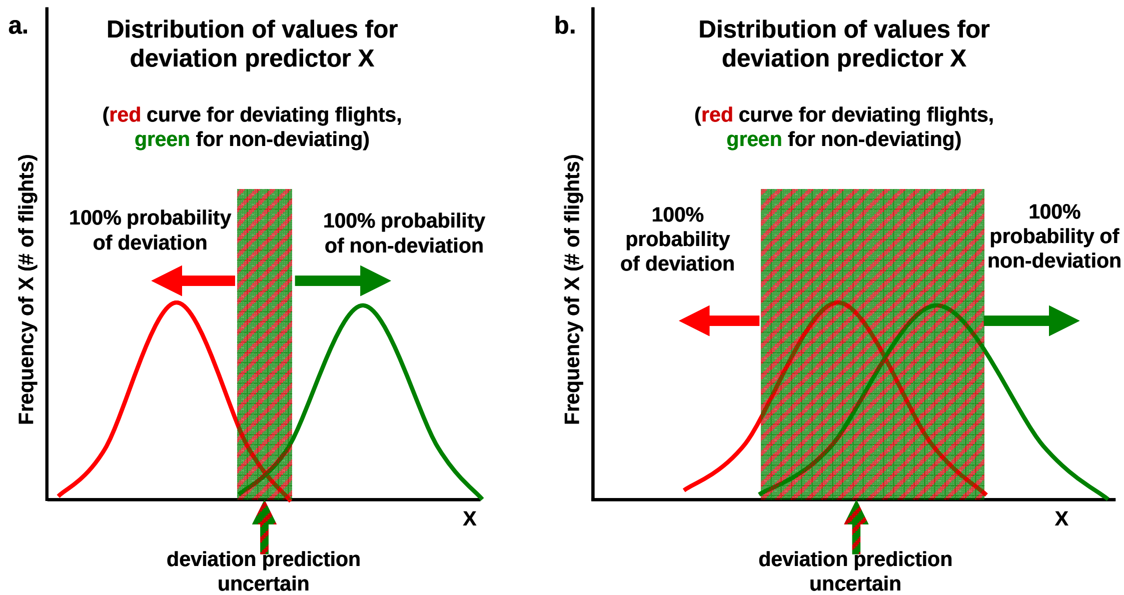


*Figure B-1. Illustration of predictor strength. Figure (a) illustrates a good predictor. The distribution of predictor data values for deviations and non-deviations is widely separated, so there is only a small set of predictor values where there is uncertainty about the outcome so the prediction error is small. Figure (b) illustrates a poor predictor, where there is significant overlap between the two distributions.*

Three sets of deviation modeling experiments were performed. Table B1 lists the predictor inputs and best predictors (the combination of predictors that resulted in the lowest prediction error, in order of predictor strength) for 20 experiments that included VIL, echo top and lightning inputs; Figure B2 is the corresponding error output plot (repeated from Figure 8a in the main text). Note that the best predictor in the 11 models with the lowest prediction errors is deltaZ, using a 90$^{th}$ percentile measurement (from either the 16 or 60 km scale) of echo tops. (Predictors are defined in Table A2.).

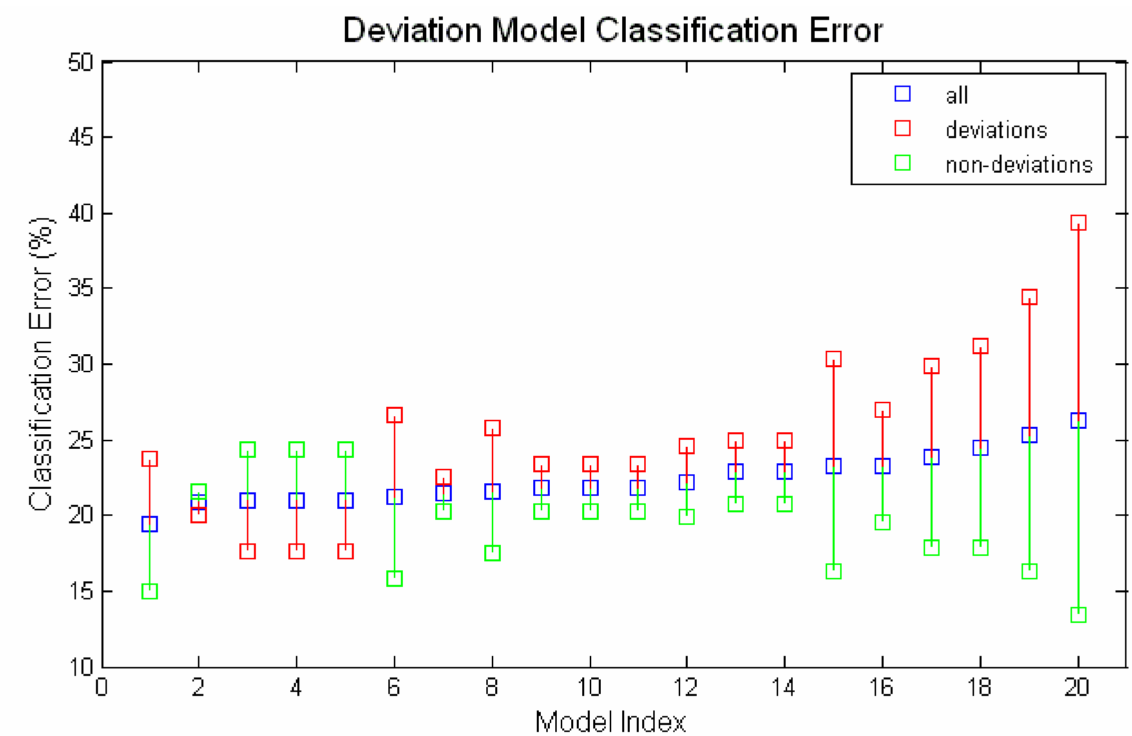


*Figure B-2. Deviation prediction errors corresponding to Table B1.*

Table B2 and Figure B3 summarize the models from the 6 echo top and lightning experiments. Note that the performance of the best of these models is comparable to the best models using both echo top and VIL predictors. However, there is a larger difference between the prediction error for deviations and non-deviations in the echo tops-only model.

Table B3 and Figure B4 summarize the VIL and lightning experiments. The best VIL-only models have prediction error rates that are approximately 25% higher than those from echo tops and VIL or echo tops-only models.

**TABLE B-1**

**Summary of deviation prediction model experiments, using VIL, echo top and lightning as predictors**

| Plot index | VIL inputs | | Echo top inputs | | Lightning (60 km) | Best predictors (in order of predictive power) |
|---|---|---|---|---|---|---|
| | 16 km | 60 km | 16 km | 60 km | | |
| 1 | vilpain_16 | vil90_60 | dzet90_16 | et40_60 | lght_60 | dzet90_16, vil90_60 |
| 2 | vilpain_16 | vil90_60 | et30avg_16 | dzet90_60 | lght_60 | dzet90_60, vil90_60, et30avg_16, lght_60 |
| 3 | vil90_16 | l3pct_60 | et30avg_16 | dzet90_60 | lght_60 | dzet90_60, l3pct_60, lght_60, et30avg_16 |
| 4 | vil3avg_16 | l3pct_60 | et30avg_16 | dzet90_60 | lght_60 | dzet90_60, l3pct_60, lght_60, et30avg_16 |
| 5 | vilpain_16 | l3pct_60 | et30avg_16 | dzet90_60 | lght_60 | dzet90_60, lght_60, et30avg_16, l3pct_60 |
| 6 | vilpain_16 | vil90_60 | etpain_16 | dzet90_60 | lght_60 | dzet90_60, vil90_60, etpain_16 |
| 7 | vil3avg_16 | l3pct_60 | etpain_16 | dzet90_60 | lght_60 | dzet90_60, vil3avg_16, etpain_16 |
| 8 | vil90_16 | l3pct_60 | etpain_16 | dzet90_60 | lght_60 | dzet90_60, vil90_16, etpain_16 |
| 9 | vil90_16 | l3pct_60 | dzet90_16 | et40_60 | lght_60 | dzet90_16, l3pct_60 |
| 10 | vil3avg_16 | l3pct_60 | dzet90_16 | et40_60 | lght_60 | dzet90_16, l3pct_60 |
| 11 | vilpain_16 | l3pct_60 | dzet90_16 | et40_60 | lght_60 | dzet90_16, l3pct_60 |
| 12 | vil3avg_16 | l3pct_60 | et30avg_16 | et40_60 | lght_60 | et40_60, et30avg_16, lght_60, vil3avg_16 |
| 13 | vilpain_16 | l3pct_60 | et30avg_16 | et40_60 | lght_60 | et40_60, et30avg_16, lght_60, vilpain_16 |
| 14 | vilpain_16 | vil90_60 | et30avg_16 | et40_60 | lght_60 | et30avg_16, et40_60, lght_60, vilpain_16 |
| 15 | vil90_16 | l3pct_60 | et30avg_16 | et40_60 | lght_60 | lght_60, et30avg_16, et40_60 |
| 16 | vilpain_16 | l3pct_60 | etpain_16 | dzet90_60 | lght_60 | dzet90_60, lght_60 |
| 17 | vil3avg_16 | l3pct_60 | etpain_16 | et40_60 | lght_60 | etpain_16, vil3avg_16 |
| 18 | vilpain_16 | vil90_60 | etpain_16 | et40_60 | lght_60 | etpain_16, vil90_60 |
| 19 | vil90_16 | l3pct_60 | etpain_16 | et40_60 | lght_60 | etpain_16, vil90_16, et40_60 |
| 20 | vilpain_16 | l3pct_60 | etpain_16 | et40_60 | lght_60 | etpain_16, et40_60 |

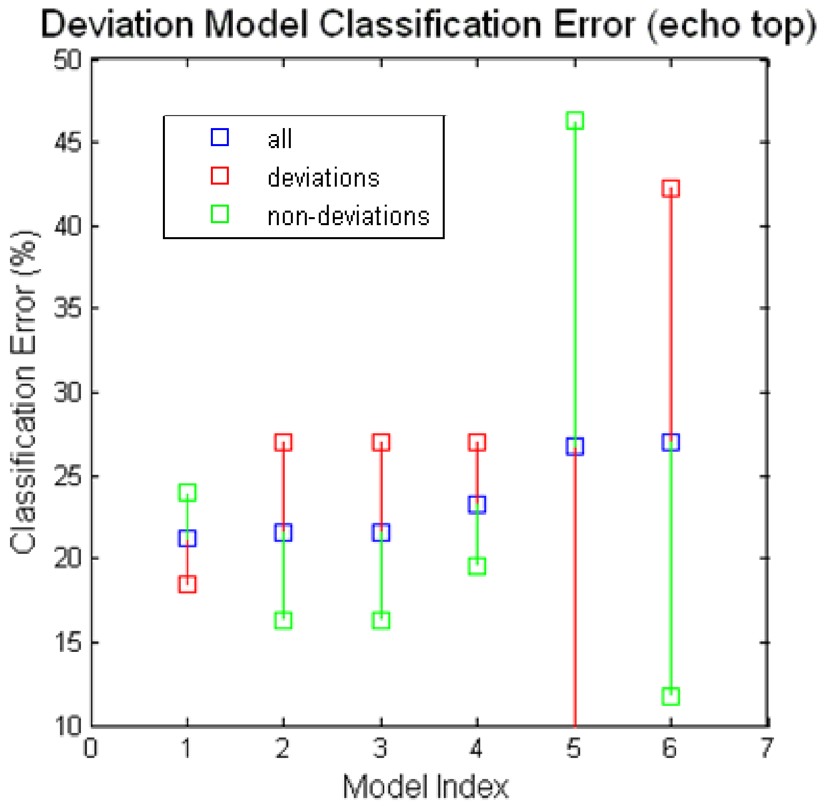


*Figure B-3. Deviation prediction errors corresponding to Table B2.*

**TABLE B-2**

**Summary of deviation prediction model experiments, using echo tops and lightning as predictors**

| Plot index | Echo top inputs | | Lightning (60 km) | Best predictors (in order of predictive power) |
|---|---|---|---|---|
| | 16 km | 60 km | | |
| 1 | et30avg_16 | dzet90_60 | lght_60 | dzet90_16, lght_60, et30avg_16 |
| 2 | dzet90_16 | et40_60 | lght_60 | dzet90_16, lght_60 |
| 3 | dzet90_16 | dzet90_60 | lght_60 | dzet90_16, lght_60 |
| 4 | etpain_16 | dzet90_60 | lght_60 | dzet90_60, lght_60 |
| 5 | et30avg_16 | et40_60 | lght_60 | et40_60, et30avg_16 |

| | | | | |
|---|---|---|---|---|
| 6 | etpain_16 | et40_60 | lght_60 | et40_60, lght_60 |

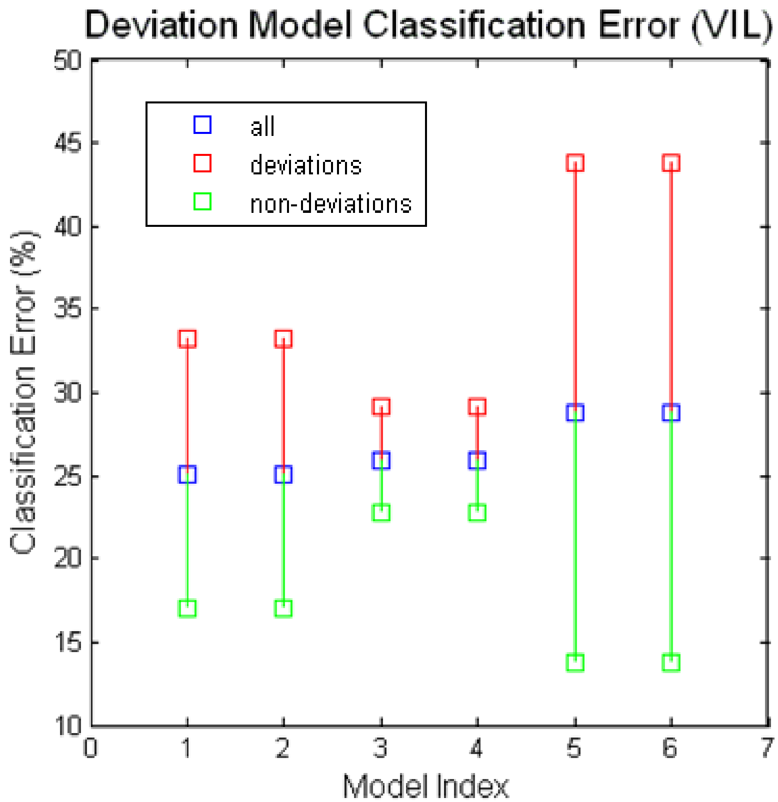


*Figure B4 Deviation prediction errors corresponding to Table B3.*

**TABLE B-3**

**Summary of deviation prediction model experiments, using VIL and lightning as predictors**

| Plot index | VIL inputs | | Lightning (60 km) | Best predictors (in order of predictive power) |
|---|---|---|---|---|
| | 16 km | 60 km | | |
| 1 | vil3avg_16 | vil90_60 | lght_60 | vil3avg_16, lght_60 |
| 2 | vil3avg_16 | l3pct_60 | lght_60 | vil3avg_16, lght_60 |
| 3 | vil90_16 | vil90_60 | lght_60 | vil90_16, lght_60 |
| 4 | vil90_16 | l3pct_60 | lght_60 | vil90_16, lght_60 |
| 5 | vilpain_16 | vil90_60 | lght_60 | lght_60, vilpain_16 |
| 6 | vilpain_16 | l3pct_60 | lght_60 | lght_60, vilpain_16 |

# APPENDIX C
# CONVECTIVE FEATURE BOUNDARIES AND DETERMINATION OF AVOIDANCE DISTANCE

Table C1 defines the weather features referenced in the avoidance distance distribution box plot (Figure C1). The box plots in Figure C1 show the minimum, $25^{th}$ percentile, median, $75^{th}$ percentile and maximum avoidance distance observer for each feature in the 220 deviations examined. Note that all the weather features examined were not present in all the convective cells presumed to cause the deviations. For example, only 129 cells contained a region where VIL >= level 2 and echo tops >= 40 kft (weather feature index 3).

Figure C1 indicates that the avoidance distances for VIL level 2, 3 and 4 convective cell boundaries (weather features 1, 6 and 11, respectively) are the most consistent; that is, the spread between the $25^{th}$ and $75^{th}$ percentiles is the smallest. This suggests that one may be able to identify convective cells that pilots wish to avoid using the deviation prediction model, define the boundary of the convective cell(s) as the VIL level 2 or 3 contour that encloses them and determine acceptable trajectories using the avoidance distance. However, it must be stressed that these results are very preliminary and based upon a very small sampling of flights. More research is needed to validate and refine these concepts.

**TABLE C-1**

**Weather features contour boundaries used to define avoidance distances for deviating trajectories**

| Weather feature index | Feature contour | Weather feature index | Feature contour |
|---|---|---|---|
| 1 | VIL = level 2 | 13 | VIL = level 4 & echo top = 40 kft |
| 2 | VIL = level 2 & echo top = 30 kft | 14 | VIL = level 4 & echo top = 50 kft |
| 3 | VIL = level 2 & echo top = 40 kft | 15 | VIL = level 4 & echo top = flight altitude |
| 4 | VIL = level 2 & echo top = 50 kft | 16 | VIL = level 5 |
| 5 | VIL = level 2 & echo top = flight altitude | 17 | VIL = level 5 & echo top = 30 kft |
| 6 | VIL = level 3 | 18 | VIL = level 5 & echo top = 40 kft |
| 7 | VIL = level 3 & echo top = 30 kft | 19 | VIL = level 5 & echo top = 50 kft |
| 8 | VIL = level 3 & echo top = 40 kft | 20 | VIL = level 5 & echo top = flight altitude |
| 9 | VIL = level 3 & echo top = 50 kft | 21 | echo top = 30 kft |
| 10 | VIL = level 3 & echo top = flight altitude | 22 | echo top = 40 kft |
| 11 | VIL = level 4 | 23 | echo top = 50 kft |
| 12 | VIL = level 4 & echo top = 30 kft | 24 | echo top = flight altitude |

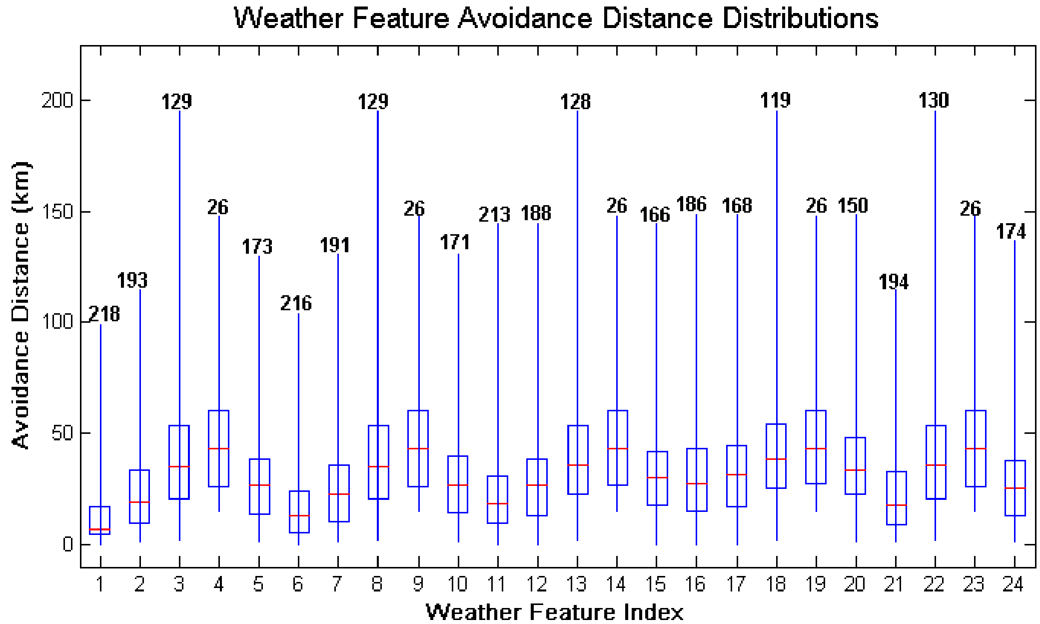


*Figure C1. Distribution of weather feature avoidance distances. Numbers at the top of each box plot indicate how many convective cells associated with pilot deviations included the weather feature whose avoidance distance is plotted in the box plot. So, for example, 129 out of 220 convective cells contained a region where VIL >= level 2 and echo tops >= 40 kft (plot index 3); the median avoidance distance from the boundary of that region was ~40 km (red line inside the box).*

# GLOSSARY

| | |
|---|---|
| ATC | Air Traffic Control |
| CCA | Convectively Constrained Area |
| CCFP | Collaborative Convective Forecast Product |
| CIWS | Corridor Integrated Weather System |
| ETMS | Enhanced Traffic Management System |
| FAA | Federal Aviation Administration |
| NEXRAD | Next Generation Weather Radar |
| SAU | Strategic Airspace Usage |
| VIL | Vertically Integrated Liquid |
| VIP | Video Integrator and Processor |

## REFERENCES


1. FAA Aeronautical Information Manual, Feb. 17, 2005.

2. Rhoda, D.A., E.A. Kocab, M.L. Pawlak, 2002: "Aircraft encounters with convective weather in en route vs. terminal airspace above Memphis, Tennessee", 10th Conference on Aviation, Range and Aerospace Meteorology, American Meteorological Society, Portland, OR.

3. Robinson, M. J., J.E. Evans, B.A. Crowe, 2002: "En Route Weather Depiction Benefits of the NEXRAD Vertically Integrated Liquid Water Product Utilized by the Corridor Integrated Weather System", 10th Conference on Aviation, Range and Aerospace Meteorology, American Meteorological Society, Portland, OR.

4. Robinson, M. J., Evans, B. Crowe, D. Klingle-Wilson, S. Allan, 2004: "Corridor Integrated Weather System Operational Benefits 2002-2003: Initial Estimates of Convective Weather Delay Reduction", MIT Lincoln Laboratory Project Report ATC-313.

5. Troxel, S.D., and C.D. Engholm, 1990: "Vertical reflectivity profiles: Averaged storm structures and applications to fan beam radar weather detection in the U.S.", 16th Conference on Severe Local Storms, American Meteorological Society, Kananaskis Park, Alta, Canada.

6. Smalley, D., B. Bennett and M. Pawlak, 2003: "New Products for the NEXRAD ORPG to Support FAA Critical Systems", Long Beach, CA, 19th American Meteorological Society International Conference on Interactive Info Processing Systems for Meteorology, Oceanography and Hydrology.

7. DeLaura, R., and S. Allan, 2003: "Route Selection Decision Support in Convective Weather: A Case Study of the Effects of Weather and Operational Assumptions on Departure Throughput", Budapest, Hungary, 5th Eurocontrol/FAA ATM R&D Seminar ATM-2003, http://atm2003.eurocontrol.fr/.

8. Mahoney, J., S. Seseske, J.E. Hart, M.P. Kay, and B.G. Brown, 2004: "Defining Observation Fields for Verification of the Collaborative Convective Forecast Product (CCFP)): Part 2", Proceedings of the American Meteorological Society 11th Conference on Aviation, Range and Aerospace Meteorology, Hyannis, MA.

9. Lippmann, R.P., L. Kukolich and E. Singer, 1993: "LNKnet Neural Network Machine Learning, and Statistical Software for Pattern Classification", The Lincoln Laboratory Journal, Vol. 6, No. 2.

10. Williams, E.R., M.E. Weber and R.E. Orville, 1989: “The Relationship Between Lightning Type and Convective State of Thunderstorms”, Journal of Geophysical Research, Vol. 94, No. D11, pp. 13,213-13,220.

11. Carey, L.D. and S.A. Rutledge, 1996: “A multiparameter radar case study of the microphysical and kinematic evolution of a lightning producing storm”, Meteorology and Atmospheric Physics, Vol. 59, pp. 33-64.